
Mesoscopic simulations of polyelectrolyte electrophoresis in nanochannels

Jens Smiatek¹ and Friederike Schmid²

¹ Institut für Physikalische Chemie, Westfälische Wilhelms-Universität Münster, D-48149 Münster jens.smiatek@uni-muenster.de

² Institut für Physik, Johannes-Gutenberg Universität-Mainz, D-55699 Mainz friederike.schmid@uni-mainz.de

Summary. We present the results of mesoscopic dissipative particle dynamics (DPD) simulations of coupled electrohydrodynamic phenomena on the micro- and nanoscale. The effects of electroosmotic flow and slippage combined with polyelectrolyte electrophoresis are investigated in detail, taking full account of hydrodynamic and electrostatic interactions. Our numerical results are in excellent agreement with analytical calculations.

1 Introduction

Microfluidic devices like bio-MEMS (micro-electronical-mechanical-systems) and bio-NEMS (nano-electronical-mechanical-systems) have attracted broad interest over the last years due to their huge potential in biotechnology. The flow profiles in such micro- or nanosized devices are strongly influenced by the properties of the boundaries due to the large surface-to-volume ratio in these systems. Surface characteristics like the wetting behavior and/or slippage have a dramatic effect on the microscopic flow, leading to sometimes unexpected behavior.

One particularly important mechanism is electroosmotic transport: in contact with a liquid, many materials commonly used in nanotechnology (*e.g.*, polydimethylsiloxane (PDMS)) become charged due to ionizations of surface groups [Isr91]. As a consequence, surfaces are often covered by a compensating counterion layer [Hun89]. In an external electric field, the ions are driven in one direction, dragging the surrounding solvent with them. As a result, a flow is induced in the fluid, the electroosmotic flow (EOF). This electrokinetic effect has numerous consequences. For example, it alters drastically the migration dynamics of mesoscopic objects like polyelectrolytes or colloids [Vio00]. In microchannels, the EOF generated at the channel walls induces a total net flow, which is technologically attractive because it can be controlled and manipulated more easily on the submicrometer scale than pressure- or shear-driven flow.

One important application of microchannels is to separate different fragments of biological matter like DNA by their length for sequencing or further manipulation. High molecular weight polyelectrolytes cannot be separated by naive electrophoresis

in free salt solution due to the fact that the electrophoretic mobility becomes length independent for long chains [Vio00]. In many separation methods, the polyelectrolytes are driven through micro- or nanostructured environments to overcome this problem, *e.g.*, a disordered gel (in gel electrophoresis), or structured microchannels. The presence of boundaries alters the dynamical behavior of the macromolecules drastically [MMT07], and their dynamical behavior results from a complex interplay of electrostatics, hydrodynamics, and confinement effects on the molecules.

Our research focuses on the investigation of the explicit coupling of electrohydrodynamic effects in the nanometer scale in confined geometries by coarse-grained mesoscopic simulations [SSH09, SS10]. We use Dissipative Particle Dynamics (DPD), which is a popular mesoscopic method in mesoscopic simulations. The results for polyelectrolyte electrophoresis in small microchannels are related to the experiments published by Mathé *et al.* in [MMT07]. In particular, we investigate in detail the influence of the electroosmotic flow on the total polyelectrolyte mobility. We find an excellent agreement between theory and numerical results.

2 Dissipative Particle Dynamics

Dissipative Particle Dynamics (DPD) was originally developed by Hoogerbrugge and Koelman [HK92] as a combination of Lattice Gas Automata characteristics and Molecular Dynamics methods. Compared to atomistic Molecular Dynamics simulations, this method gives access to much longer time- and length scales and is therefore suited to study the long-time behaviour of soft matter systems and transport phenomena. It is coarse-grained, momentum-conserving, and creates a well-defined canonical ensemble.

The basic DPD equations are given by the forces on one particle, which involve two-particle interactions that are given by

$$\mathbf{F}_i^{DPD} = \sum_{i \neq j} \mathbf{F}_{ij}^C + \mathbf{F}_{ij}^D + \mathbf{F}_{ij}^R \quad (1)$$

with a conservative force \mathbf{F}_{ij}^C

$$\mathbf{F}_{ij}^C = -\nabla_{ij} U_{ij}(r_{ij}), \quad (2)$$

a dissipative force \mathbf{F}_{ij}^D which reads

$$\mathbf{F}_{ij}^D = -\gamma_{DPD} \omega_D(r_{ij}) (\hat{r}_{ij} \cdot \mathbf{v}_{ij}) \hat{r}_{ij} \quad (3)$$

with the friction coefficient γ_{DPD} and an additional random force \mathbf{F}_{ij}^R yielding

$$\mathbf{F}_{ij}^R = \sigma \omega_R(r_{ij}) \check{\zeta}_{ij} \hat{r}_{ij}. \quad (4)$$

where the weighting function is given by

$$\omega_D(r_{ij}) = [\omega_R(r_{ij})]^2 \equiv \omega_{DPD}(r_{ij}), \quad (5)$$

such that a canonical ensemble is sampled at equilibrium [GW97, EW95]. In DPD simulations, the conservative forces are often taken to have a certain soft shape [GW97]. Here we only use the DPD *thermostat* as described above. The random

number $\check{\zeta}$ has zero mean and unit variance and is symmetric, $\check{\zeta}_{ij} = \check{\zeta}_{ji}$, to ensure the conservation of momentum and the weighting function is arbitrary and often chosen linear [GW97]. It depends on the interparticle distance r_{ij} and the cut-off radius r_c . The strength of the interaction is steered by the distance of the particles with

$$\omega_{DPD}(r_{ij}) = \begin{cases} 1 - \frac{r_{ij}}{r_c} & : r_{ij} < r_c \\ 0 & : r_{ij} \geq r_c \end{cases} \quad (6)$$

while the amplitude of the Gaussian white noise in Eqn. (4) is given by

$$\sigma^2 = 2\gamma_{DPD}k_B T \quad (7)$$

with the Boltzmann constant k_B and the temperature T . Eqn. (1) can be integrated by an ordinary Molecular Dynamics integration scheme like the Velocity-Verlet algorithm [FS01] which is used in the ESPResSo package.

3 The software package ESPResSo

All simulations in this work have been carried out using extensions of the software package ESPResSo (An **E**xtensible **S**imulation **P**ackage for **R**esearch on **S**oft matter) [AML05]. ESPResSo was mainly developed for coarse-grained mesoscopic simulation approaches. One of the advantages of this program is its high performance MPI-parallelization implemented for simulations on supercomputers. Users can furthermore change and extend the program code to adopt it for their own purposes. ESPResSo incorporates several simulation techniques like Lattice-Boltzmann, Dissipative Particle Dynamics, Stochastic Dynamics as well as pure Molecular Dynamics techniques. Another feature are the several implemented electrostatic algorithms like MMM1D, MMM2D, MMM3D, P3M, ELC and screened Debye-Hückel potentials, which allow to choose between the fastest calculation methods available. In summary, ESPResSo provides a well founded basis code for high performance computing on parallel clusters. The steering of the simulations is based on a TCL (Tool Command Language) script. For starting a simulation, no explicit knowledge of implementation details is needed. Even newcomers in the methods of computer simulations can successfully run a simulation after a short time.

Several tools for analysis are additionally included in the program. ESPResSo is under public license and free to download [AML05]. Users that develop new ideas are invited to submit their source code, written in the programming language C to be incorporated after testing in the newest release version. The development of ESPResSo continues and a number of extensions is already planned.

We ran our simulations on the NEC SX-8 Cluster at the High Performance Computing Center Stuttgart. The number of computing nodes has normally been chosen to 4 which corresponds to 32 CPUs. Each job has got a typical runtime of 4 hours by using the concept of setting checkpoints.

4 Polyelectrolyte electrophoresis in microchannels

4.1 General theory

We consider for simplicity a planar slit channel with identical walls at $z = \pm L/2$, exposed to an external electric field E_x in the x direction. The electrostatic potential

$\Phi(x, y, z)$ then takes the general form $\Phi(x, y, z) = \psi(z) + E_x x + \text{const.}$ where we can set $\psi(0) = 0$ for simplicity. The electrolyte in the channel is taken to contain n different ion species i with local number density $\rho_i(z)$ and valency Z_i , which results in a net charge density $\rho(z) = \sum_{i=1}^n (Z_i e) \rho_i(z)$. The electric field then generates a force density $f_x(z) = \rho(z) E_x$ in the fluid. Comparing the Poisson equation for the electrostatic potential ψ ,

$$\frac{\partial^2 \psi(z)}{\partial z^2} = -\frac{\rho(z)}{\epsilon_r} \quad (8)$$

(where ϵ_r is the dielectric constant), with the Stokes equation

$$\eta_s \frac{\partial^2 v_x(z)}{\partial z^2} = -f_x(z) = -\rho(z) E_x \quad (9)$$

(with the shear viscosity η_s), one finds immediately $\partial_{zz} v_x(z) = \partial_{zz} \psi(z) (\epsilon_r E_x / \eta_s)$. For symmetry reasons, the profiles v_x and ψ must satisfy the boundary condition $\partial_z v_x|_{z=0} = \partial_z \psi|_{z=0} = 0$ at the center of the channel. This gives the relation

$$v_x(z) = \frac{\epsilon_r E_x}{\eta_s} \psi(z) + v_{\text{EOF}}, \quad (10)$$

where we have used $\psi(0) = 0$ and identified the fluid velocity at the center of the channel with the EOF velocity, $v_x(0) = v_{\text{EOF}}$. We further define $\psi_B := \psi(\pm z_B)$ (for no-slip boundaries, ψ_B is the so-called Zeta-Potential [Hun89, SS10]).

The roughness of the channel boundaries is included in the partial slip boundary condition.

$$\delta_B \partial_z v(x)|_{z_B} = v_x(z)|_{z_B}, \quad (11)$$

where $v_x(z)$ denotes the component of the velocity in x-direction evaluated at the position z_B of the so-called ‘‘hydrodynamic boundary’’. This boundary condition is characterized by two effective parameters, namely (i) the slip length δ_B and (ii) the hydrodynamic boundary z_B . We note that the latter does not necessarily coincide with the physical boundary. Inserting the partial-slip boundary condition for the flow, Eqn. (11), we finally obtain the following simple expression for the electroosmotic mobility,

$$\mu_{\text{EOF}} = v_{\text{EOF}} / E_x = \mu_{\text{EOF}}^0 (1 + \kappa \delta_B), \quad (12)$$

where we have defined the inverse ‘surface screening length’

$$\kappa := \mp \frac{\partial_z \psi}{\psi} \Big|_{z=\pm z_B}, \quad (13)$$

and μ_{EOF}^0 is the well-known Smoluchowski result [Hun89] for the electroosmotic mobility at sticky walls,

$$\mu_{\text{EOF}}^0 = -\epsilon_r \psi_B / \eta_s. \quad (14)$$

The remaining task is to determine the screening parameter κ . If the surface charges are very small and the ions in the liquid are uncorrelated, it can be calculated analytically within the linearized Debye-Hückel theory [Isr91]. The Debye-Hückel equation for the evolution of the potential ψ in an electrolyte solution reads $\partial_{zz} \psi = \kappa_D^2 \psi$ with the inverse Debye-Hückel screening length

$$\kappa_D = \sqrt{\frac{\sum_{i=1}^n (Z_i e)^2 \rho_{i,0}}{\epsilon_r k_B T}}, \quad (15)$$

where $\rho_{i,0}$ is the density of ions i far from the surface. It is solved by an exponentially decaying function,

$$\psi(z) \propto (e^{\kappa_D z} + e^{-\kappa_D z} - 2). \quad (16)$$

Inserting that in Eq. (13), one finds $\kappa = \kappa_D$, *i.e.*, the surface screening length is identical with the Debye screening length.

Unfortunately, the range of validity of the Debye-Hückel theory is limited, it breaks down already for moderate surface potentials ψ_B and/or for highly concentrated ion solutions. Nevertheless, the exponential behavior often persists even in systems where the Debye-Hückel approximation is not valid. For high ion concentrations a Debye-Hückel-type approximation can still be used in a wide parameter range, if κ_D is replaced by a modified effective screening length [BKN05]. For high surface charges, analytical solutions are again available in the so-called 'strong coupling limit', where the profiles are predicted to decay exponentially with the Gouy-Chapman length [MN01]. This limit is very special and rarely encountered. At intermediate coupling regimes, the decay length must be obtained empirically, *e.g.*, by fitting the charge distribution $\rho(z)$ to an exponential behavior, which is characterized by the same exponential behavior than $\psi(z)$ by virtue of the Poisson equation,

$$\sum_{i=q}^n (Z_i e) \rho_i(z) \propto \frac{\partial^2 \psi(z)}{\partial z^2} \propto (e^{\kappa z} + e^{-\kappa z}). \quad (17)$$

Assuming that the electrophoretic velocity of the polyelectrolyte

$$v_p(x) = \mu_e E_x \quad (18)$$

is influenced by the electroosmotic mobility of the counterions μ_{EOF} , a total mobility has to be defined $\mu_t = \mu_{EOF} + \mu_e$ which describes the overall mobility of the electrophoretic object. Putting everything together, the total net electrophoretic mobility μ_t of a polyelectrolyte in the channel can be expressed in terms of the electroosmotic mobility μ_{EOF} as

$$\frac{\mu_t}{\mu_{EOF}} = 1 + \frac{\mu_e}{\mu_{EOF}^0 (1 + \kappa \delta_B)}, \quad (19)$$

where the ratio μ_e/μ_{EOF}^0 depends only weakly on the ionic strength of the electrolyte and the slip length of the surface. The main effect of slippage is incorporated in the factor $(1 + \kappa \delta_B)^{-1}$ [SS10].

4.2 Simulation details

We have studied the electrophoresis of a single charged polymer of length $N = 20$ in electrolyte solutions, confined by a planar slit channel with charged walls. All particles, polymer, solvent and ions, are modeled explicitly. We use a simulation box of size $(12\sigma \times 12\sigma \times 10\sigma)$ which is periodic in x - and y -direction and confined by impermeable walls in the z -direction. The walls repel the particles *via* a soft repulsive WCA potential of range σ and amplitude ϵ . (Hence the accessible channel width for the particles is actually $L_z = 8\sigma$). Ions and monomers repel each other with the same WCA potential. In addition, chain monomers are connected by harmonic springs

$$U_{harmonic} = \frac{1}{2} k (r_{ij} - r_0)^2 \quad (20)$$

with the spring constant $k = 25\epsilon/\sigma^2$ and $r_0 = 1.0\sigma$. Neutral solvent particles have no conservative interactions except with the walls. The wall contains immobilized, negatively charged particles at random positions. Every second monomer on the polyelectrolyte with 20 beads carries a negative charge resulting in 10 charged monomers. The solvent contains the positive counterions for the walls and the polyelectrolyte, and additional (positive and negative) salt ions. All charges are monovalent, and the system as a whole is electroneutral. In addition to their other interactions, charged particles interact *via* a Coulomb potential with the Bjerrum length $\lambda_B = e^2/4\pi\epsilon_r k_B T = 1.0\sigma$, and they are exposed to an external field $E_x = -1.0\epsilon/e\sigma$. Specifically, we have studied systems with a surface charge density of $\sigma_A = -0.208e\sigma^{-2}$ which corresponds to 30 charged particles per wall. In a recent publication [SSH09], we have shown that this corresponds to the ‘weak-coupling regime’, *i.e.*, the regime where the Poisson-Boltzmann theory is valid. The electrostatic coupling constant [MN01] $\Xi = 2\pi Z^3 \lambda_B^3 \sigma_A$ ($Z = 1$ is the valency of the cations), which gives the strength of electrostatic interactions between the surface and the ions compared to thermal energy, is close to unity, $\Xi \sim 1.3$. In this earlier work, we have also studied the effect of using homogeneously charged wall instead of discrete embedded charge, and found the differences to be negligible [SSH09]. The use of discrete embedded charges has practical advantages in our simulation code, which is why we use them here. The total counterion density was $\rho = 0.06\sigma^{-3}$ and the salt density varied between $\rho_s = 0.05625, 0.0375, 0.03, 0.025,$ and $0.015\sigma^{-3}$. In molar units, this corresponds to 0.272, 0.181, 0.145, 0.121 and 0.072 mol/l, if we identify $\lambda_B \approx 0.7$ nm, *i.e.*, the Bjerrum length in water at room temperature [Vio00].

We use DPD simulations with a friction coefficient $\gamma_{\text{DPD}} = 5.0\sigma^{-1}(m\epsilon)^{1/2}$. (More precisely, we only use the DPD *thermostat*, not the soft conservative DPD forces. All conservative forces in our system are either WCA forces, spring forces, or Coulomb forces as explained above). The density of the solvent particles was $\rho = 3.75\sigma^{-3}$, and the temperature of the system was $T = 1.0\epsilon/k_B$. For these parameters, the shear viscosity of the DPD fluid – as determined by fitting the amplitude of Plane Poiseuille flows [SAF08] – is given by $\eta_s = (1.334 \pm 0.003)\sigma^{-2}(m\epsilon)^{1/2}$. The DPD timestep was $\delta t = 0.01\sigma(m/\epsilon)^{1/2}$.

Tunable-slip boundary conditions were used with friction coefficients $\gamma_L = 0.1, 0.25, 0.5, 0.75, 1.0,$ and $6.1\sigma^{-1}(m\epsilon)^{1/2}$. The range of the viscous layer was $z_c = 2.0\sigma$. Only the solvent particles interact with the tunable-slip boundaries. By performing Plane Poiseuille and Plane Couette flow simulations with the above given parameters, the slip length δ_B and the hydrodynamic boundary positions z_B can be determined independently [SAF08]. The hydrodynamic boundary position is found at $|z_B| = (3.866 \pm 0.266)\sigma$ in all simulations.

4.3 Results

Polyelectrolytes in absence of external fields

To understand the behaviour of polyelectrolytes in salty solution we first studied the dynamics in absence of external fields. The general theory [Vio00] implies that hydrodynamic interactions between the monomers are important to describe the dynamic behaviour adequately. This results in the so called Zimm dynamics [Vio00]. If external electric fields are present, hydrodynamic interactions between the charged

monomers are screened due to the presence of salt. The two rivaling effects which are the electrophoresis of the polyelectrolyte as well as the electroosmosis of the mobile counterions in opposite direction lead to a crucial screening of hydrodynamic interactions which is described by Rouse dynamics [Vio00].

A powerful tool to investigate the underlying dynamics in experiments as well as in computer simulations is given by the dynamic version of the structure factor which is defined by

$$S(\mathbf{k}, t) = \frac{1}{N} \sum_{i,j} \langle e^{i\mathbf{k}(\mathbf{R}_i(t) - \mathbf{R}_j(t_0))} \rangle \quad (21)$$

with the actual monomer position \mathbf{R}_i respectively \mathbf{R}_j . For the inverse length scale $1/R_g \ll k \ll 1/a_0$ with the gyration radius R_g [DE86] and the smallest microscopic length a_0 and the finite time interval $t_b \ll t \ll \tau$ after the ballistic time t_b and the longest relaxation time τ , the dynamic structure factor obeys the following scaling relation [DK93]

$$S(k, t) = S(k, 0)f(k^z t) \quad (22)$$

which depends on the parameter z . This parameter differentiates between the different regimes. For the Zimm dynamics it is given by

$$z = 3 \quad (\text{Zimm-Regime}) \quad (23)$$

and for Rouse dynamics

$$z = 2 + 1/\nu \quad (\text{Rouse-Regime}) \quad (24)$$

with the Flory parameter ν which describes the inverse fractal dimension of the polyelectrolyte [DE86].

We have compared an uncharged polymer and a half charged polyelectrolyte in a salt solution of concentration $\rho_s = 0.05\sigma^{-3}$ and a solvent density of $\rho = 3.0\sigma^{-3}$ with free periodic boundary conditions in all dimensions. All the other parameters are in agreement to the above described simulation details. Fig. 1 presents our simulation results for an uncharged chain and the polyelectrolyte. Our results indicate that although external fields are absent, polyelectrolytes can be described best by Rouse dynamics whereas uncharged polymers can be described by Zimm dynamics. More results on that topic can be found in [Smi09, SS08].

Polyelectrolyte electrophoresis in microchannels

In this section our numerical results are presented which indicate the drastic influence of the electroosmotic flow on the total mobility of the polyelectrolyte. Larger slip lengths even enhance this effect.

Fig. 2 presents the results of the ionic distribution for a salt concentration of $\rho_s = 0.05625\sigma^{-3}$ and a counterion density of $\rho = 0.0525\sigma^{-3}$ with a surface ion density of $\sigma_s = 0.208\sigma^{-2}$ in presence of the polyelectrolyte. Due to the large number of cations in comparison to the anions, the cation density in the middle of the channel is increased (inset of Fig. (2)). Calculating the ionic difference $\Delta\rho = \rho_c - \rho_a$ as the difference of the cationic and anionic density yields

$$\frac{\partial^2}{\partial z^2} \psi(z) = - \sum_i^N \frac{Z_i e}{\epsilon} \rho_i(z) = - \frac{Ze}{\epsilon} \Delta\rho \quad (25)$$

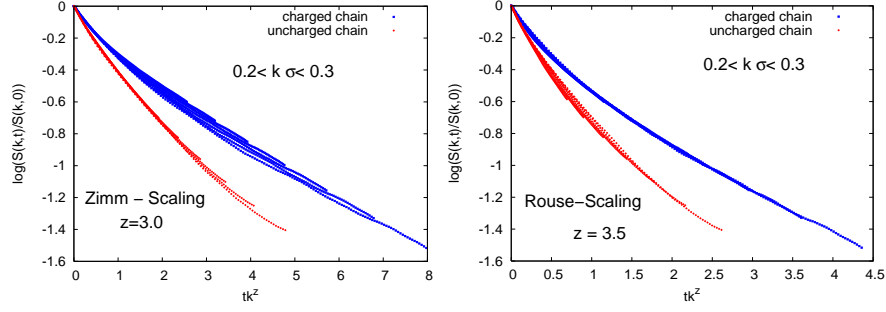


Fig. 1. Dynamic structure factor $S(k,t)$ for an uncharged chain (red) in correspondence to a half charged chain (blue) for $0.2 < k\sigma < 0.3$ and salt concentration $\rho_s = 0.05\sigma^{-3}$. The timescale for the uncharged chain is $0 < t/\tau < 180$ in contrast to $0 < t/\tau < 300$ for the half charged polyelectrolyte. Both chains consist of $N = 50$ monomers. Left side: Zimm-scaling with $z = 3$. Right side: Rouse-scaling with $z = 3.5$.

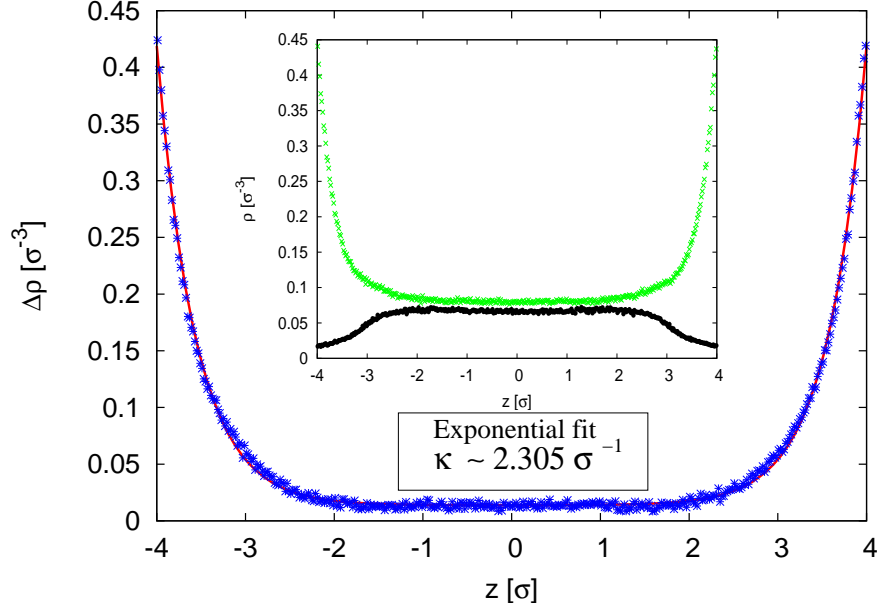


Fig. 2. Distribution of the ionic difference $\Delta\rho = \rho_c - \rho_a$ for an exemplary salt concentration of $\rho_s = 0.05625\sigma^{-3}$ with a surface ion density of $\sigma_s = 0.208\sigma^{-2}$. The red line corresponds to the exponential fit of Eqn. (26) with an effective inverse screening length of $\kappa = 2.305 \pm 0.025\sigma^{-1}$. **Inset:** Distribution of cations (salt cations and counterions) with green symbols and anions (salt anions) with black symbols for an the exemplary salt concentration for the above given parameters.

Table 1. Fitted inverse screening lengths κ for the different salt concentrations ρ_s and a fixed counterion density of $\rho = 0.0525\sigma^{-3}$.

$\rho_s[\sigma^{-3}]$	$\kappa[\sigma^{-1}]$
0.015	1.996 ± 0.041
0.0225	2.011 ± 0.049
0.03	1.983 ± 0.041
0.0375	2.182 ± 0.047
0.05625	2.305 ± 0.025

with the unique valency $|Z|$ [SS10]. As we have mentioned in section 4, the application of the Debye-Hückel theory for non electroneutral bulk systems is not valid and has to be replaced by an effective inverse screening length κ . Thus we have used the following fit function

$$\Delta\rho = \Delta\rho_0(e^{-\kappa z} + e^{\kappa z}) + c \quad (26)$$

to determine the effective inverse screening length κ , with the fit parameters $\Delta\rho_0$, c and κ_D . The red line in Fig. 2 shows that the fit describes the ionic difference adequately. The fitted parameter values of κ for the different salt concentrations are presented in Tab.1. Significant differences between the inverse screening lengths are only observed for salt concentrations $\rho_s \geq 0.0375\sigma^{-3}$. Thus, for lower salt concentrations, the screening of electrostatic interactions is mainly effectuated by the much larger number of counterions instead of the salt ions [SS10].

The corresponding electroosmotic flow profiles for an exemplary salt concentration of $\rho_s = 0.05625\sigma^{-3}$ are shown in Fig. 3. The different magnitudes correspond to varying slip lengths. Larger slip lengths enhance the flow profile drastically. All points are in good agreement to the integrated analytical expression of Eqn. (26) in terms of the Stokes equation (9) with partial-slip boundary conditions. Thus the description of the electroosmotic flow in terms of the Stokes theory is valid.

Fig. 4 compiles our numerical results for the electroosmotic mobility for all salt concentrations and slip lengths. They are in very good agreement to the theoretical prediction of Eqn. (12), where $\mu_{0,EOF}$ has been determined independently by a linear regression for each salt concentration. It is worth noting that the presence of the polyelectrolyte does not perturb the amplitude of the electroosmotic flow.

After investigating the electroosmotic flow of the solvent, we focus on the dynamics of the polyelectrolyte. The monomer distribution for a salt concentration of $\rho_s = 0.05625\sigma^{-3}$ is presented in Fig. 5. The fit shows that the distribution is dominated by a peak in the middle of the channel with a variance of $Var \sim 2.28\sigma$. Thus the main drag of the electroosmotic flow on the polyelectrolyte is exerted in the middle of the channel, and the rapid variations of the electroosmotic flow in close vicinity to the boundaries (Fig. 3) have little influence on the polyelectrolyte mobility. Estimating the total mobility by assuming a constant plug-like flow profile

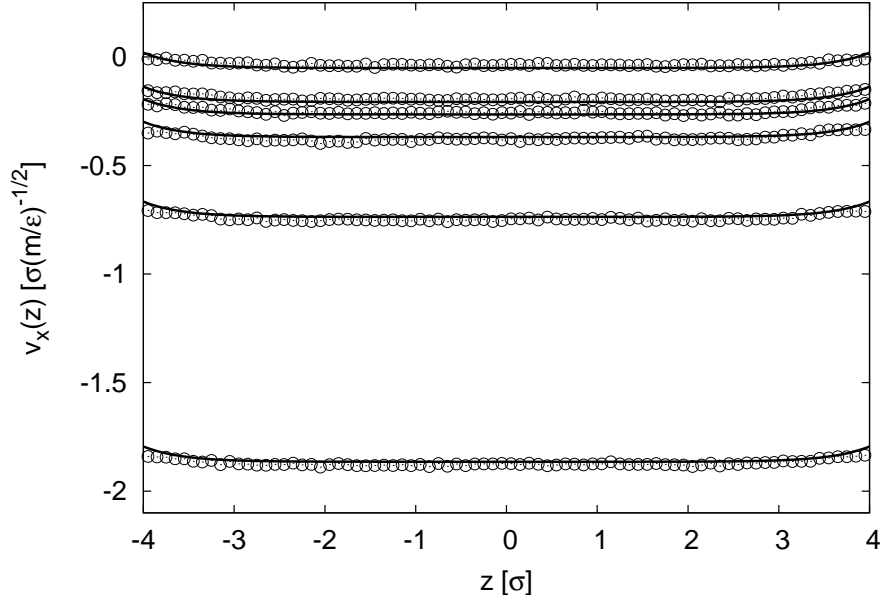


Fig. 3. Exemplary flow profiles for a salt concentration $\rho_s = 0.05625\sigma^{-3}$ for varying slip lengths (from bottom to top: $\delta_B = (14.98, 5.66, 2.63, 1.77, 1.29, 0.00)\sigma$.) The black lines are the integrated theoretical predictions in terms of the Stokes equation (9) with a fitted inverse screening length of $\kappa = 2.305\sigma^{-1}$.

for the fluid in the middle of the channel from $z = -1.52\sigma$ to $z = 1.52\sigma$ due to the variance of the monomer distribution therefore seems reasonable.

The influence of the electroosmotic flow on the polyelectrolyte can be investigated by regarding static properties like the radius of gyration $R_g^2 = (1/2N^2) \sum_{i,j=1}^N \langle (\mathbf{R}_i - \mathbf{R}_j)^2 \rangle$ and the end-to-end radius with $R_e^2 = \langle (\mathbf{R}_N - \mathbf{R}_1)^2 \rangle$ [DE86]. The

Table 2. Radius of gyration R_g and end to end radius R_e for a polyelectrolyte with $N = 20$ monomers for different salt concentrations ρ_s .

$\rho_s[\sigma^{-3}]$	$R_g[\sigma]$	$R_e[\sigma]$
0.015	3.2218 ± 0.047	10.6480 ± 0.0314
0.0225	3.1661 ± 0.0041	10.2736 ± 0.0266
0.03	3.1486 ± 0.0451	10.1777 ± 0.0292
0.0375	3.1279 ± 0.0045	10.0819 ± 0.0287
0.05625	3.0825 ± 0.0045	9.8331 ± 0.0280

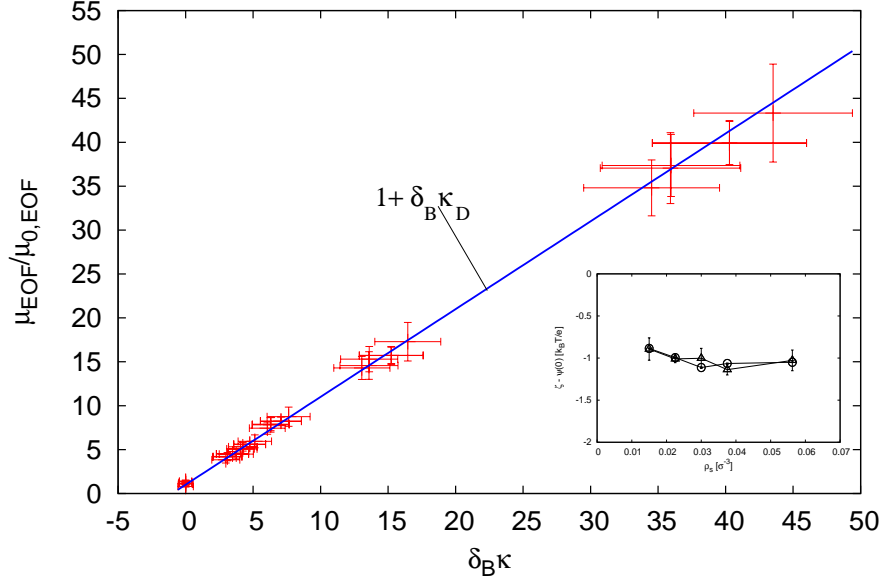


Fig. 4. Ratio $\mu_{EOF}/\mu_{0,EOF}$ plotted against $\delta_B \kappa$ for the different salt concentrations and screening lengths given in Tab. 1 with counterions of density $\rho = 0.0525\sigma^{-3}$. The blue line is the theoretical prediction of Eqn. (12) with slope $1 + \delta_B \kappa_D$.

values of these parameters are shown in Tab. 2. Both properties decrease with larger salt concentration due to a more pronounced screening of electrostatic interactions which is in accordance to standard theories [Vio00]. Although the values for the end to end radius are quite large, in all cases the box dimensions in the unconfined directions with $b_{x,y} = 12\sigma$ are larger than the maximal average extension of the chain. Possible explanations for these large ratios between the end-to-end and gyration radii could be shear-induced elongation [BKN05] or direct squeezing due to the presence of the channel walls.

The total mobility of the polyelectrolyte for varying boundary conditions is finally presented in Fig. 6. The theoretical prediction of Eqn. (19) is in good agreement with the numerical results with the fitted ratio $\mu_e/\mu_{EOF}^0 = -3.778 \pm 0.128$. With no-slip boundaries ($\delta_B \approx 0$) one obtains ordinary behaviour where the polyelectrolyte migrates in opposite direction to the electroosmotic flow. In the presence of slip, the absolute mobility may become negative if the amplitude of the electroosmotic flow exceeds a critical value given by a combination of the inverse screening and slip lengths, and if the sign of the wall charges is identical to the net charge of the polyelectrolyte. If the wall is oppositely charged to the polyelectrolyte, slippage effects should even enhance the total velocity of the polyelectrolyte.

The right inset of Fig. 6 shows the total displacement of the chains center of mass for various slip lengths and a salt concentration of $\rho_s = 0.05625\sigma^{-3}$. In nearly all cases except for $\delta_B \approx 0$, the total mobility of the polyelectrolyte is negative with $|\mu_p| \ll |\mu_{EOF}|$, indicating negative values of μ_t/μ_{EOF}^0 . This can only be explained

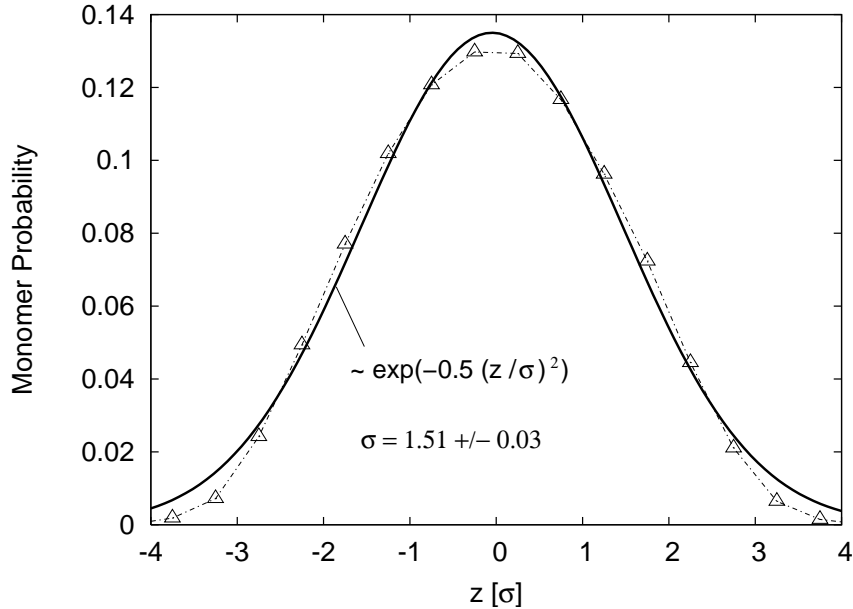


Fig. 5. Monomer appearance probability inside the channel for a salt concentration of $\rho_s = 0.05625\sigma^{-3}$.

in terms of the drag force of the electroosmotic flow and the surplus of cations in close vicinity to the boundaries (Fig. 2) and is in agreement to the results derived above.

To summarize, the assumptions and calculations of section 4 are in good agreement to the presented numerical results in this section. The total mobility of the polyelectrolyte can therefore be adequately described by Eqn. (19).

5 Summary

We have presented mesoscopic DPD simulations of polyelectrolyte electrophoresis in narrow microchannels, taking full account of hydrodynamic and electrostatic interactions. We have shown that the product of the inverse screening length κ and the slip length δ_B massively influences the electroosmotic flow and therefore the total mobility of the polyelectrolyte. Thus the characteristics of the boundaries have to be taken into account for a proper description of the polyelectrolyte migration dynamics. For certain parameter sets, even a negative mobility can be achieved. All our numerical results are in good agreement to the analytical derived results.

In summary, only a combination of electroosmotic, electrophoretic, electrostatic and slippage effects does describe the total mobility of polyelectrolytes in microchannels adequately. Our simulations indicate and explain total negative mobilities due to boundary effects which also have been observed in recent experiments [MMT07]. The characteristics of the channel walls could be used to significantly enhance flow

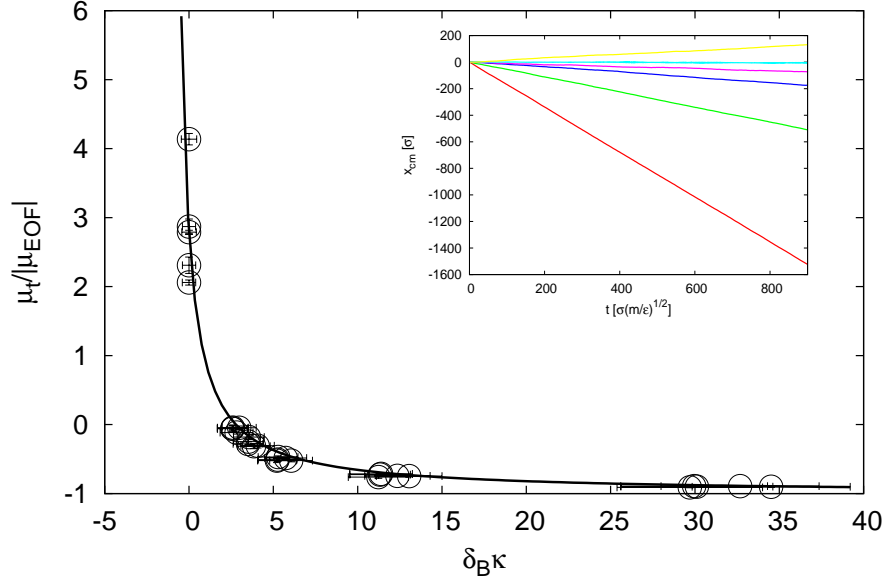


Fig. 6. Ratio $\mu_t/|\mu_{EOF}|$ plotted against $\delta_B \kappa$ for all salt concentrations. The black line is the theoretical prediction of Eqn. (19) with absolute values of $|\mu_{EOF}|$. In the limit $\delta_B \kappa \rightarrow \infty$, the total mobility of the polyelectrolyte is equal to the electroosmotic flow. The ratio μ_p/μ_{EOF}^0 has been fitted to -3.778 ± 0.128 . Negative values of $\mu_t/|\mu_{EOF}|$ indicate absolute negative total mobilities of the polyelectrolyte. **Inset:** Total displacement of the polyelectrolytes center of mass for different boundary conditions and a salt concentration of $\rho_s = 0.05625\sigma^{-3}$. The total mobility becomes negative if the relation $|\mu_e| \ll |\mu_{EOF}|$ is fulfilled. The lines correspond from top to bottom to the slip lengths $\delta_B \approx (0.00, 1.292, 1.765, 2.626, 5.664, 14.98)\sigma$. Thus larger slip lengths indirectly enhance the total mobility of the polyelectrolyte.

profiles which offers the possibility to reduce the time needed for polymer migration or separation techniques. This could be an important aspect for future applications in microchannels or micropumps to accelerate the measuring time in experiments.

6 Acknowledgements

We thank Christian Holm, Burkhard Dünweg, Ulf D. Schiller, Marcello Sega, Michael P. Allen and Kai Grass for nice and fruitful discussions. Furthermore we thank the HLRS in Stuttgart for computing time and the Volkswagen Stiftung for funding.

References

- [Isr91] Israelachvili, J.: Intermolecular and Surface Forces. Academic Press, London (1991)
- [Hun89] Hunter, R. J.: Foundations of Colloid Science, Vol.1. Clarendon Press, Oxford (1991)
- [Vio00] Viovy, J.-L.: Electrophoresis of DNA and other polyelectrolytes: Physical mechanisms. *Rev. Mod. Phys.*, **72**, 813–872 (2000)
- [MMT07] Mathe, J., Di Meglio, J. -M., Tinland, B.: Electrophoretic separation of large DNAs using steric confinement. *J. Colloid Interface Sci.*, **316**, 831–835 (2007)
- [SSH09] Smiatek, J., Sega, M., Holm, C., Schiller, U. D., Schmid, F.: Mesoscopic simulations of the counterion-induced electroosmotic flow: a comparative study. *J. Chem. Phys.*, **24**, 244702–244710 (2009)
- [HK92] Hoogerbrugge, P. J., Koelman, J. M. V. A.: Simulating microscopic hydrodynamic phenomena with dissipative particle dynamics. *Europhys. Lett.*, **19**, 155–160, (1992)
- [GW97] Groot, R. D., Warren, P. B.: Dissipative particle dynamics: Bridging the gap between atomistic and mesoscopic simulation. *J. Chem. Phys.*, **107**, 4423–4435 (1997)
- [EW95] Español, P., Warren, P. B.: Statistical mechanics of dissipative particle dynamics. *Europhys. Lett.*, **30**, 191–195 (1995)
- [FS01] Frenkel, D., Smit, B.: Understanding Molecular Simulation. 2nd Edition. Academic Press, San Diego CA (2008)
- [AML05] Arnold, A., Mann, B. A., Limbach, H.-J., Holm, C.: ESPResSo: An extensible simulation package for research on soft matter systems. *Comp. Phys. Comm.*, **174**, 704–727 (2005)
- [SS10] Smiatek, J., Schmid, F.: Polyelectrolyte electrophoresis in nanochannels: a dissipative particle dynamics simulation. *J. Phys. Chem. B.*, **114**, 6266–6272 (2010)
- [BKN05] Boroudjerdi, H., Kim, Y. -W., Naji, A., Netz, R. R., Schlagberger X., Serr A.: Statics and Dynamics of Strongly Charged Soft Matter. *Phys. Rep.*, **416**, 129–199 (2005)
- [MN01] Moreira, A. G., Netz, R. R.: Binding of similarly charged plates with counterions only. *Phys. Rev. Lett.*, **87**, 078301–078305 (2001)
- [HE81] Hockney, R. W., Eastwood, J. W.: Computer simulation using Particles. McGraw-Hill, New York (1981)
- [SAF08] Smiatek, J., Allen, M. P., Schmid, F.: Tunable-slip boundaries for coarse-grained simulations of fluid flow. *Eur. Phys. J. E*, **26**, 115–123 (2008)
- [DE86] Doi, M. Edwards S. F.: The Theory of Polymer Dynamics. Oxford Press, Oxford (1986)
- [DK93] Dünweg, B., Kremer, K.: Molecular dynamics simulation of a polymer chain in solution. *J. Chem. Phys.*, **99**, 6983–6998 (1993)
- [Smi09] Smiatek, J.: Mesoscopic simulations of electrohydrodynamic phenomena. PhD thesis, Bielefeld University (2009)
- [SS08] Smiatek, J., Scherer, C., Schmid, F., manuscript in preparation